International Journal of General Medicine

Dovepress
Taylor & Francis Group

Open Access Full Text Article

ORIGINAL RESEARCH

Uncovering the Interplay of Ferroptosis and Immune System in Coronary Artery Disease: Construction and Validation of a Diagnostic Model

Zhiyong Zhang, Xiaoming Zhu, Tao Zhang, Chuang Li, Dapeng Zhang, Weiming Li, Lin Zhao

Heart Center and Beijing Key Laboratory of Hypertension, Beijing Chaoyang Hospital, Capital Medical University, Beijing, 100020, People's Republic of China

Correspondence: Lin Zhao, Heart Center and Beijing Key Laboratory of Hypertension, Beijing Chaoyang Hospital, Capital Medical University, No. 8 Gongti South Road, Chaoyang District, Beijing, 100020, People's Republic of China, Email trichina2007@126.com

Objective: To explore the roles of ferroptosis and immune regulation in coronary artery disease (CAD) and find potential diagnostic biomarkers.

Methods: Three gene expression profile datasets were used, with GSE202625 as the training set and GSE42148 and GSE180081 as validation sets. LIMMA identified differentially expressed genes (DEGs) between CAD and control groups. ClusterProfiler conducted functional enrichment analysis. Ferroptosis-related genes from FerrDb were intersected with DEGs. ssGSEA and Pearson analysis analyzed immune cell subsets. LASSO built a diagnostic model. In vitro and in vivo experiments included qPCR, ELISA, pathological examination, and Western blot.

Results: In the GSE202625 dataset, 70 genes were upregulated and 895 genes were downregulated in CAD samples. A total of 29 ferroptosis-associated DEGs were identified, and immune cell profiling revealed differences in immune cell subsets between CAD and healthy cohorts. LASSO identified six genes (IDH1, MMD, NDRG1, WIPI1, BID, and TRIM26) for the diagnostic model, which collectively achieved an AUC of 0.904 in the training dataset, 0.776 in the GSE180081 validation dataset, and 0.902 in the GSE42148 validation dataset. IDH1 had the highest diagnostic efficacy with an AUC of 0.821. Clinically, 26 CAD patients (angiographically confirmed, ≥50% luminal stenosis) and 12 controls showed that CAD patients had higher prevalence of hypertension, diabetes, and elevated lipid markers. IDH1 was downregulated in CAD patients and inversely correlated with the Gensini score. In the CAD mouse model, IDH1 expression was decreased in aortic tissues.

Conclusion: Six genes correlated with CAD, and the multi-gene diagnostic model performed well. IDH1 was a potential CAD biomarker, aiding CAD diagnosis and treatment research.

Keywords: coronary artery disease, ferroptosis, immune regulation, biomarkers, disease diagnosis

Introduction

Coronary Artery Disease (CAD) is a condition characterized by the development of atherosclerotic plaques within the coronary arteries, leading to insufficient blood supply to the myocardium and is one of the leading causes of mortality and morbidity.[1] The primary feature of CAD is the progressive narrowing of the arterial lumen due to the growth of atherosclerotic plaques, which impedes blood flow to the myocardium. This pathological process can manifest clinically as a spectrum of conditions, ranging from stable angina to more severe and life-threatening acute myocardial infarction.[2] CAD is a multi-factorial disease involving genetic and environmental risk factors. While lipid accumulation and inflammation are well-established mechanisms, emerging evidence highlights the role of ferroptosis and immune dysregulation in its pathogenesis, which may play a crucial yet underappreciated role in CAD.[3–7]

Ferroptosis, an iron-dependent form of lipid peroxidation-driven cell death, has been linked to atherosclerotic plaque progression and inflammatory responses in CAD.[8–11] Dysregulated iron metabolism and oxidative stress in CAD may exacerbate ferroptosis, promoting vascular cell damage.[12] Clinically, CAD patients often exhibit metabolic disorders such

Received: 1 April 2025
Accepted: 9 July 2025
Published: 15 July 2025

Graphical Abstract

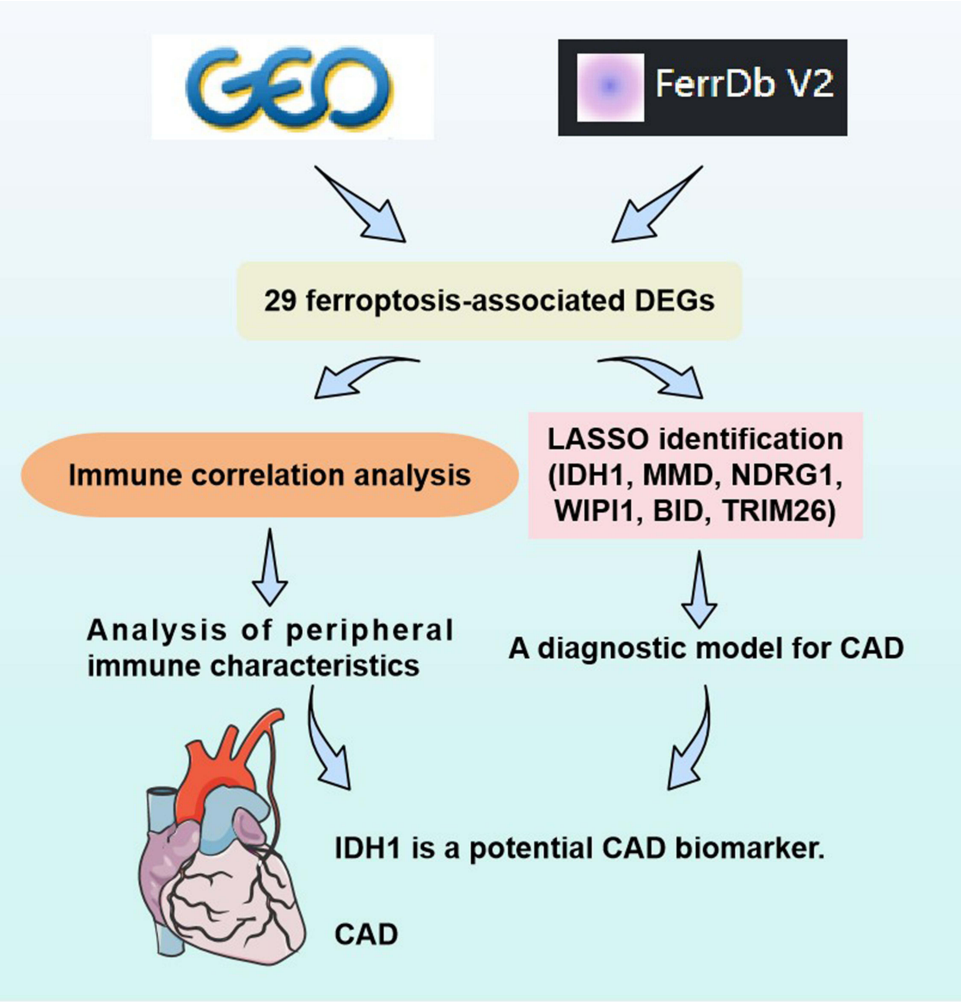

as dyslipidemia and hyperglycemia, which can affect iron metabolism through different mechanisms. For example, hyperglycemia may enhance the accumulation of intracellular iron, further promoting ferroptosis.[13] Thus, investigating the role of ferroptosis in CAD, especially the interaction between iron metabolism and oxidative stress, may provide a theoretical foundation for novel therapeutic strategies.

The immune system has been demonstrated to play a central role in the development and progression of CAD.[14] The infiltration of immune cells, such as macrophages, T cells, and neutrophils, into atherosclerotic plaques is a common feature of the disease.[15,16] These immune cells secrete a variety of cytokines and chemokines, which not only modulate the inflammatory microenvironment but also influence the proliferation, migration, and apoptosis of vascular cells.[17] Therefore, understanding the complex interplay between ferroptosis and immune responses in CAD is crucial for a deeper comprehension of the pathophysiology of the disease and the identification of potential therapeutic targets.

While ferroptosis and immune regulation are increasingly recognized in CAD, their diagnostic utility remains unclear. High-throughput technologies have enabled the analysis of large-scale gene expression datasets in CAD research.[18] Integrating bioinformatics and machine learning, we identified differentially expressed genes (DEGs) and potential biomarkers to advance CAD diagnosis. Here, we hypothesized that ferroptosis-related genes could serve as diagnostic biomarkers and intersect with immune cell profiles in CAD.

In this study, we aimed to identify ferroptosis-related diagnostic biomarkers and characterize immune cell infiltration in CAD using machine learning and network analysis. We hypothesized these genes could diagnose/prognose CAD and reveal immune interactions. Analyzing public datasets and conducting in vitro/in vivo experiments, we integrated bioinformatics and validation to clarify ferroptosis roles and advance precision strategies for CAD.

Materials and Methods

Data Collection and Processing

Three gene expression profile datasets (GSE42148, GSE180081, and GSE202625) were obtained from the Gene Expression Omnibus (GEO) database (https://www.ncbi.nlm.nih.gov/geo/), maintained by the National Center for Biotechnology Information (NCBI). The mRNA expression profile dataset GSE202625, annotated with GPL13607, was downloaded as the training cohort. This dataset comprises 52 samples, including 27 angiography-confirmed CAD samples and 25 asymptomatic control samples from the general population. All samples were derived from the whole blood of enrolled patients. The RNA single-molecule sequencing dataset GSE180081, annotated with GPL14761, was obtained as the validation cohort, containing 96 samples: 48 with mild coronary artery stenosis and 48 with moderate to severe (MID+) coronary artery stenosis. The mRNA expression profile dataset GSE42148, also annotated with GPL13607, was downloaded as an additional validation cohort, including 24 samples: 13 angiography-confirmed CAD samples and 11 asymptomatic control samples from the general population.

RNA sequencing (RNA-seq) data from GSE202625 and GSE180081 were normalized to transcripts per million (TPM). Prior to subsequent analysis, the three datasets (GSE42148, GSE180081, and GSE202625) were processed using the "sva" package to remove batch effects.

Identification of Differentially Expressed Genes (DEGs)

Based on the combined datasets, we utilized the LIMMA package to identify differentially expressed genes (DEGs) between the CAD and control groups, using a threshold of $|\log FC| > 1$ and an adjusted p-value < 0.05. Subsequently, we visualized these DEGs using volcano plots and heatmaps.

Functional Enrichment Analysis

Functional enrichment analysis was performed using the clusterProfiler package to identify the potential functions of target genes. GO (Gene Ontology) analysis elucidated the functional annotations of target genes across biological processes (BP), cellular components (CC), and molecular functions (MF). Through the Kyoto Encyclopedia of Genes and Genomes (KEGG) database, we further identified pathways involving these target genes in human biological systems based on candidate gene annotations. Both nominal and adjusted p-values were set at 0.05.

Identification and Analysis of Ferroptosis-Related Genes

Ferroptosis-related genes were obtained from the FerrDb database (http://www.zhounan.org/ferrdb/) (Zhou and Bao, 2020) for further analysis. This database curates ferroptosis-related markers and associated diseases. The intersection of these genes with differentially expressed genes (DEGs) from GSE202625 was identified for subsequent analysis. The "corrplot" package was then used to assess correlations among the ferroptosis-related genes.

Immune Cell Subset Analysis

To better understand the composition of immune cells in the peripheral blood of healthy individuals and CAD patients, we compared the differences in immune cell subsets between the two groups. Using single-sample gene set enrichment analysis (ssGSEA), we evaluated the differential composition of 28 immune cell types. Pearson correlation analysis was employed to reveal the correlations between immune cell distribution and differentially expressed (DE) ferroptosis-related gene expression.

Establishment and Evaluation of Diagnostic Models

Using feature selection, we applied the Least Absolute Shrinkage and Selection Operator (LASSO) regression algorithm for dimensionality reduction and identified 14 iron-related genes (IRGs) to construct a diagnostic model for CAD. We then plotted receiver operating characteristic (ROC) curves for the 14 biomarkers using training and validation datasets and calculated the area under the curve (AUC) with R software to evaluate the diagnostic performance of individual genes. Similarly, ROC analysis was performed on the combined 14 differentially expressed IRGs to assess their diagnostic value in both training and validation datasets.

Study Population

Between January 2024 and September 2024, 26 patients diagnosed with CAD via coronary angiography and 12 healthy controls were enrolled in this study at the hospital. The inclusion criteria for CAD patients were: (a) age ≥ 18 years; (b) CCTA showing obstructive stenosis in a single coronary artery (stenosis of ≥ 50% in luminal diameter). The exclusion criteria included: (a) ST-segment elevation myocardial infarction (STEMI); (b) CCTA indicating stenosis of all three major coronary arteries < 50%; (c) CCTA showing stenosis of 2 or 3 coronary arteries ≥ 50%; (d) PCI performed in multiple vessels; (e) previous coronary artery bypass grafting (CABG); (f) history of malignant tumors.

The study complied with the Helsinki Declaration and was approved by the Ethics Committee of Beijing Chaoyang Hospital. All participants provided written informed consent prior to their involvement in the study.

Clinical Data Collection

Clinical data, including general information and biochemical parameters, were collected from all participants. General information encompassed age, gender, history of hypertension, history of diabetes, smoking status, alcohol consumption habits, and body mass index (BMI). Blood pressure was measured using a standardized sphygmomanometer. Fasting blood samples were collected from all subjects for laboratory testing. An automated biochemical analyzer was used to determine the levels of serum white blood cell count (WBC), alanine aminotransferase (ALT), aspartate aminotransferase (AST), lactate dehydrogenase (LDH), triglycerides (TG), total cholesterol (TC), low-density lipoprotein cholesterol (LDL-C), and high-density lipoprotein cholesterol (HDL-C).

Gensini Score

Coronary angiography was performed on CAD patients to assess the severity of coronary artery lesions. The Gensini score was calculated based on the degree of coronary artery stenosis and the site of the lesion. Stenosis degrees were categorized as follows: ≤25% scored 1 point, 26–50% scored 2 points, 51–75% scored 4 points, 76–90% scored 8 points, 91–99% scored 16 points, and 100% scored 32 points. Weighting factors for different lesion sites were as follows: left main coronary artery, 5 points; proximal left anterior descending or circumflex artery, 2.5 points; mid left anterior descending artery, 1.5 points; distal left anterior descending artery, posterior descending artery, mid and distal circumflex artery, obtuse marginal artery, and right coronary artery, 1 point each; other small branches, 0.5 points. The Gensini score for each patient was the sum of all lesion scores, with higher scores indicating more severe CAD symptoms.

Quantitative Reverse Transcription PCR

RNA was extracted from aortic tissues of healthy controls and patients with CAD using the EZ-press RNA Purification Kit (EZBioscience Co., Ltd, China). Complementary DNA (cDNA) was synthesized using the PrimeScript™ RT Reagent Kit (Takara, Japan). The expression levels of six ferroptosis-related genes (WIPI1, TRIM26, NDRG1, MMD, IDH1, and BID) were detected by polymerase chain reaction (PCR). RT-qPCR reactions were performed on a real-time PCR system (7500, Applied Biosystems) using the TB Green Premix Ex Taq Kit (Takara, Japan), with a reaction mixture consisting of 10 μL TB Green, 0.5 μL forward primer, 0.5 μL reverse primer, 0.4 μL ROX II, 4 μL ddH_2O, and 4.6 μL cDNA sample. Primer sequences are listed in Table 1. PCR products were analyzed by agarose gel electrophoresis, with the gene GAPDH serving as an endogenous control. The relative expression levels of the genes were calculated using the 2^(-ΔΔCt) method.

Table 1 Comparison of General Data Between CAD Group and Normal Group

Variable	Normal Group (n = 12)	CAD Group (n = 26)	*P*-value
Age	63.42±10.39	69.45±12.74	0.001
Gender, male (%)	7(58.3)	14(53.8)	0.24
Hypertension, case (%)	8(66.7)	20(76.9)	0.042
Smoking, case (%)	4(33.3)	7(26.9)	0.067
Diabetes, case (%)	2(13.3)	9(34.6)	0.005
Drinking, case (%)	2(13.3)	6(23.1)	0.056
BMI (kg/m2)	24.96±3.15	26.28±5.13	0.047
Gensini score	0.0(0.00, 6.00)	22(13.4, 37.5)	0.000

Notes: Kidney function data were not routinely recorded, Pharmacological therapy data were partially available and not systematically documented in this retrospective analysis. Other comorbidities were not systematically documented.

Construction of CAD Mouse Model

Twelve 7-week-old male C57BL/6J wild-type mice, weighing 18–22 g, were purchased from Beijing Huakang Biotechnology Co., Ltd. (License No.: SCXK (Beijing) 2019–0008). Prior to the experiment, the mice were acclimated for 7 days in an environment maintained at 20–26°C with 40–70% humidity and a 12-hour light-dark cycle, with ad libitum access to food and water. Mice in the CAD group were fed a high-fat diet (23% protein, 45% fat, 20% carbohydrates, 4.5 kcal/g; Product No. D12109C), whereas those in the control group received a standard diet (24.02% protein, 12.95% fat, 63.03% carbohydrates, 3.44 kcal/g). After 20 weeks, the mice were weighed, anesthetized, and blood was collected from the abdominal aorta. Aortic tissues were harvested for subsequent analysis. The animal experiment was approved by the Animal Research Committee of Beijing Chaoyang Hospital and performed in accordance with the guidelines of the National Animal Care and Ethics Institution.

Elisa

The serum concentrations of total cholesterol (TC), low-density lipoprotein cholesterol (LDL-C), and high-density lipoprotein cholesterol (HDL-C) in mice were measured using a kit from Nanjing Jiancheng Bioengineering Institute, China, according to the manufacturer's instructions.

Pathological Examination

Aortic tissues were isolated under sterile conditions and fixed in 4% paraformaldehyde for 24 hours. After trimming and placement in dehydration cassettes, the samples were processed through standard dehydration and embedding protocols to generate 4-μm paraffin sections. These sections were stained with hematoxylin and eosin (HE) following routine dewaxing with xylene. Nuclei were stained blue with hematoxylin, and cytoplasm was stained pink with eosin. Following dehydration, the sections were mounted and examined under an Olympus optical microscope (Tokyo, Japan). Additionally, the degree of collagen deposition was evaluated using a Masson's trichrome staining kit from Solarbio Life Sciences.

Western Blot

Protein extraction from aortic tissues was performed utilizing RIPA lysis buffer (Beyotime), followed by centrifugation at 12,000 rpm for 20 minutes at 4°C. Subsequently, the protein concentration was ascertained via a BCA protein assay kit (Thermo Fisher Scientific). The extracted proteins were subjected to separation by SDS-PAGE electrophoresis and subsequently electrotransferred onto a polyvinylidene fluoride (PVDF) membrane (Millipore). The membrane was incubated with the primary antibody targeting IDH1 at 4°C overnight, and thereafter incubated with a horseradish peroxidase-conjugated secondary antibody (Jackson ImmunoResearch) for 2 hours at ambient temperature. Visualization

of the proteins was achieved through the application of an ECL chemiluminescent substrate kit (Pierce). The primary antibodies employed were anti-IDH1 (product number ab230949, Abcam, 1:100000) and anti-GAPDH (Cat No. 10494-1-AP, Proteintech, 1:40,000). Quantification of the protein bands was conducted utilizing ImageJ software.

Statistical Analysis

Data analysis was conducted using SPSS 22.0 software (SPSS, USA). The results are presented as mean ± standard deviation (SD). For normally distributed data, comparisons between two groups were made using Student's *t*-test, while one-way ANOVA was employed for the analysis of multiple groups. In cases where the data were not normally distributed, a non-parametric test was utilized. A p-value of less than 0.05 was considered to indicate statistical significance. Post-hoc sample size calculation was performed using GPower 3.1. For the primary endpoint (AUC of the diagnostic model), assuming a medium effect size ($f^2 = 0.25$), $\alpha = 0.05$, and 80% power, the required sample size was estimated to be 30 cases and 30 controls. Our current sample size (26 CAD, 12 controls) meets approximately 87% of the recommended sample size for exploratory analysis. For inter-observer variability, two independent observers evaluated Gensini scores and pathological staining results, with coefficients of variation (CV) of 5.2% and 4.8%, respectively. Intra-observer variability was assessed by repeated measurements by the same observer, yielding CVs of 3.9% for Gensini scores and 3.5% for histological evaluations.

Results

Identification of Differentially Expressed mRNAs in Peripheral Blood from GSE202625 Data

In the GSE202625 dataset (27 angiography-confirmed CAD vs 25 controls), limma identified 70 upregulated and 895 downregulated genes (Figure 1A). A heatmap highlights the top 20 differentially expressed genes linked to CAD pathogenesis (Figure 1B).

Screening and Validation of Ferroptosis-Related Genes

To explore ferroptosis-related gene involvement in CAD, intersection analysis of GSE202625 DEGs and ferroptosis-driving genes identified 29 ferroptosis-associated DEGs (Figure 1C). Their expression profiles in CAD and controls are shown in

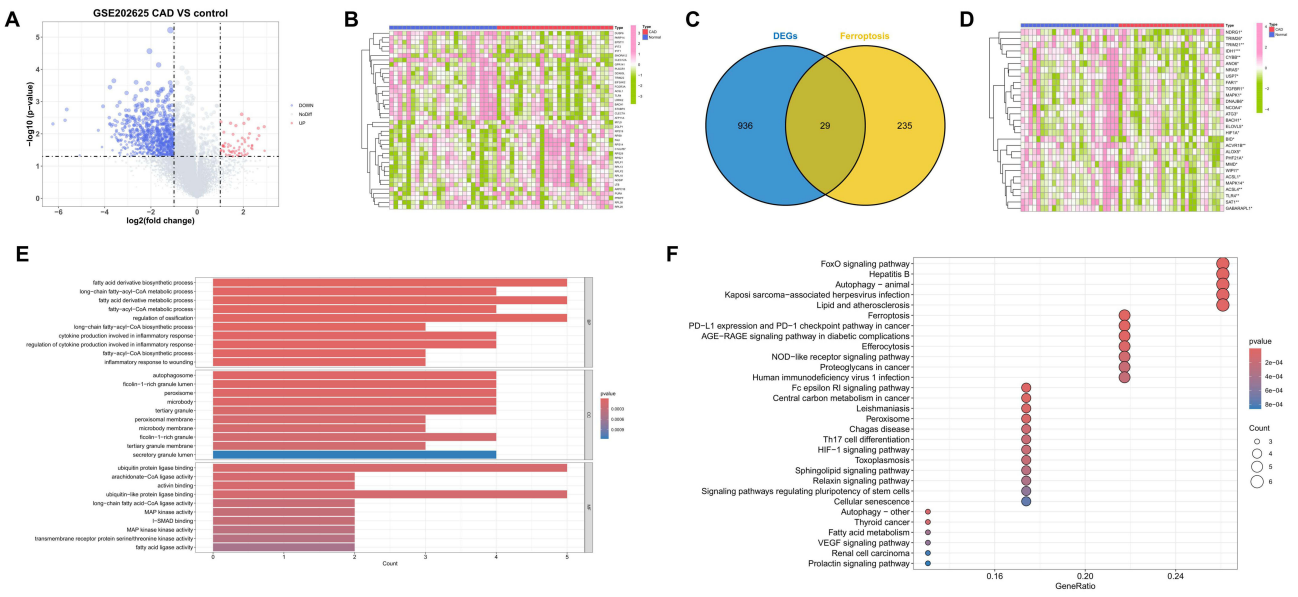

Figure 1 Screening and Analysis of Ferroptosis-related Genes. (**A**) Volcano plot of DEGs between CAD and controls. (**B**) Heatmap for the top 20 DEGs between CAD and healthy samples. Pink: Up-regulation; Green: Down-regulation. (**C**) Venn diagram of 29 DE-FRGs in CAD. (**D**) Heatmap of the expression profiles of 29 DE-FRGs in CAD and control samples. (**E**) GO analysis bar plot showed the enrichment of the DE-FRGs in BP, CC, and MF processes. (**F**) Kyoto Encyclopedia of Genes and Genomes (KEGG) pathways-gene analysis plot.

Figure 1D, with green-to-pink gradients indicating expression levels, and several genes showing significant differential expression between groups. Gene Ontology (GO) analysis indicated that these genes are predominantly involved in fatty acid metabolism, cytokine regulation, and autophagy-peroxisome functions. The interplay between dysregulated fatty acid metabolism and inflammatory processes is intricately linked to CAD pathogenesis, and autophagy-peroxisome dysfunction may potentiate endothelial injury (Figure 1E). Kyoto Encyclopedia of Genes and Genomes (KEGG) pathway analysis, highlighting the FoxO signaling pathway, ferroptosis, NOD-like receptor signaling pathway, and lipid metabolism pathways, further emphasizes their critical roles in CAD. Among these, the FoxO pathway's influence on endothelial integrity and its contribution to ferroptosis-mediated cellular damage are particularly crucial (Figure 1F).

Immune Correlation Analysis

Immune cell expression profiling unveiled pronounced disparities in the distribution of immune cell subsets between CAD and healthy cohorts. Specifically, CD56dim natural killer cells, Type 1 T helper cells, Type 17 T helper cells, and activated dendritic cells exhibited upregulated expression in CAD subjects (Figure 2A). Enrichment score box plots further elucidated that the abundance of dendritic cells and neutrophils was markedly elevated in CAD compared to the control group, implicating these immune cells as key contributors to the immunological response in CAD (Figure 2B). Additionally, a correlation matrix among diverse immune cell types revealed intricate interrelationships. Notably, a robust positive correlation was observed between activated B cells and CD4 T cells (r = 0.83), as well as between dendritic cells and natural killer cells. Conversely, the inverse correlation noted between activated B cells and CD56dim natural killer cells (r = −0.71) suggests potential antagonistic regulatory mechanisms between these cell types under specific pathophysiological contexts (Figure 2C).

LASSO Identification and Construction of Ferroptosis Diagnostic Model

Utilizing LASSO regression for dimensionality reduction, we pinpointed six genes—IDH1, MMD, NDRG1, WIPI1, BID, and TRIM26—as integral components of a diagnostic model for CAD (Figure 3A and B). Notably, IDH1

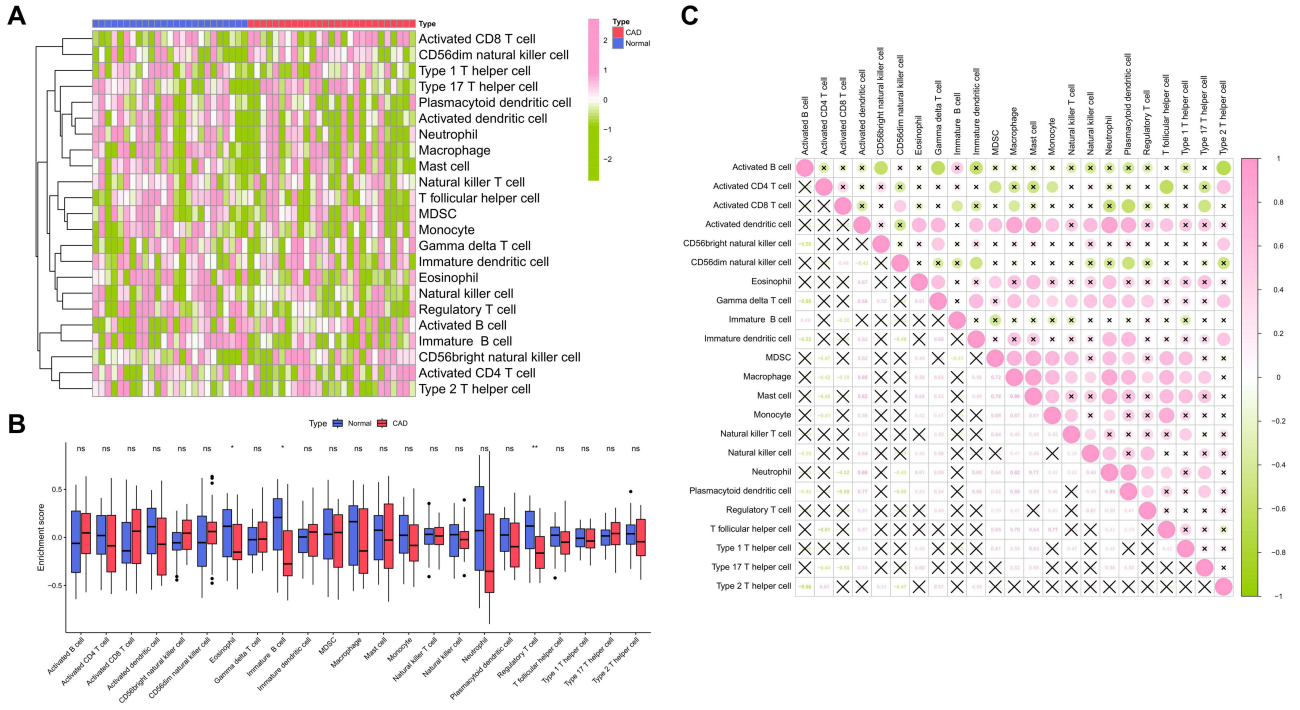

Figure 2 Immune correlation analysis. (**A**) Heatmap to show the main 28 types of immune cells changes in CAD. Pink: Up-regulation; Green: Down-regulation. (**B**) Box diagram for the enrichment score differences of the immune cells above between CAD group (Red) and normal group (Blue). (**C**) Correlation matrix highlighting the relationships between various immune cell types in CAD patients. Pink: Positive correlation; Green: Negative correlation. *p < 0.05, **p < 0.01.

https://doi.org/10.2147/IJGM.S527955

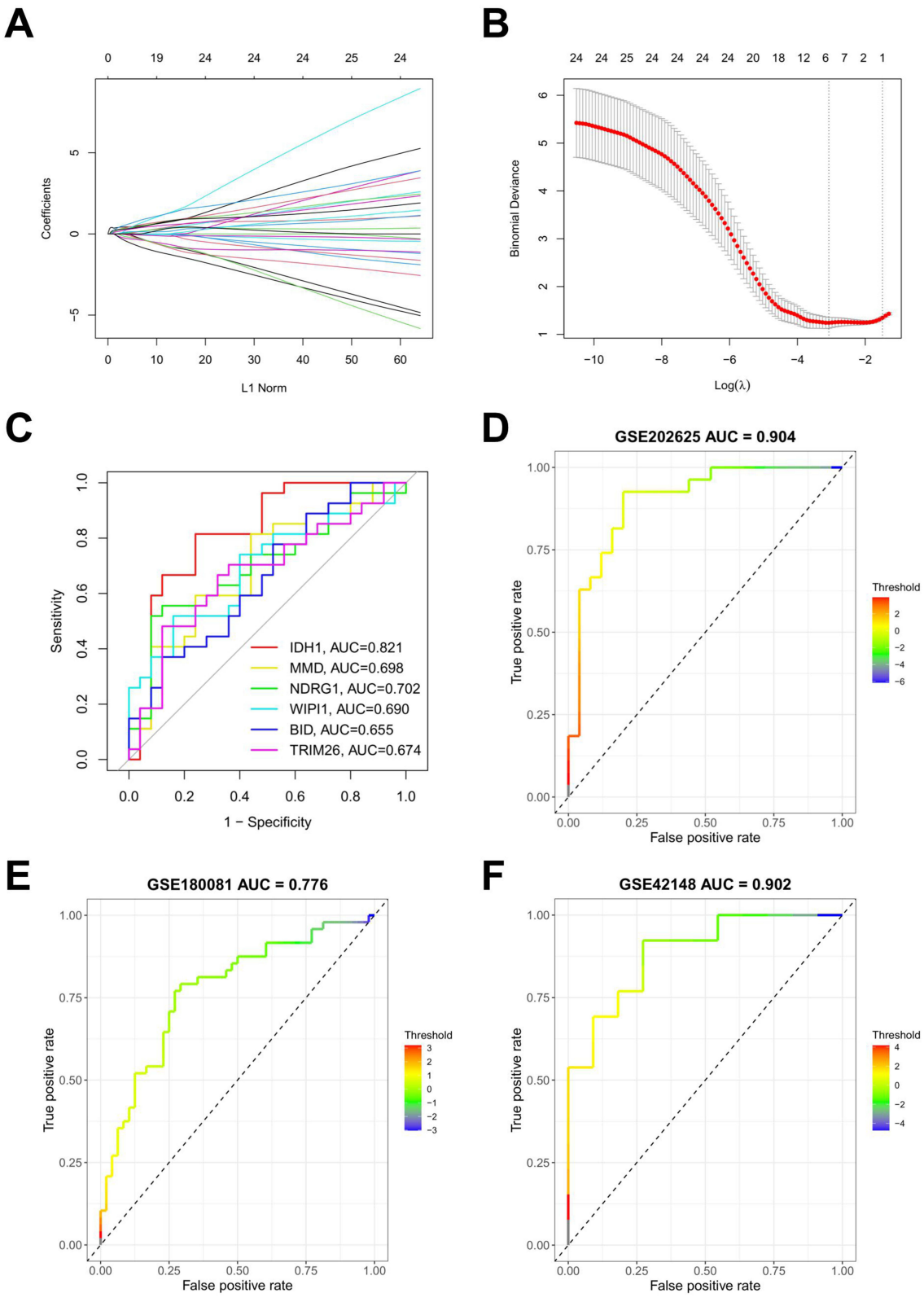

Figure 3 LASSO identification and construction of ferroptosis diagnostic model. (**A** and **B**) LASSO coefficient profiles for the selection of six key genes in the diagnostic model. (**C**) ROC curves of individual genes for CAD diagnosis. (**D–F**) ROC curves and AUC values for the diagnostic model based on the 6 ferroptosis-related genes in the GSE202625, GSE180081, and GSE42148 datasets, respectively.

demonstrated the most robust diagnostic efficacy, achieving an area under the receiver operating characteristic curve (AUC) of 0.821. The diagnostic performance of the other genes, as shown by their AUC values, was: NDRG1 (0.702), MMD (0.698), TRIM26 (0.674), WIPI1 (0.690), and BID (0.655) (Figure 3C). When integrated into a comprehensive diagnostic model, these six genes collectively achieved an AUC of 0.904 in the GSE202625 training dataset, 0.776 in the GSE180081 validation dataset, and 0.902 in the GSE42148 validation dataset (Figure 3D–F). These findings underscore the significant diagnostic potential of this ensemble of differentially expressed ferroptosis-related genes (DE-Fer), suggesting their potential as viable targets for the prevention and therapeutic intervention of CAD.

Analysis of Peripheral Immune Characteristics in CAD Patients

Among individuals with CAD, a cohort of six salient peripheral genes associated with ferroptosis exhibited substantial expression modifications. Notably, certain genes were downregulated, such as IDH1, MMD, WIPI1, and TRIM26, whereas others, including NDRG1 and BID, showed no significant changes (Figure 4A). Furthermore, these genes demonstrated unique intercorrelations. A robust positive association was observed between BID and MMD ($r = 0.74$), suggesting a potential cooperative role. The correlation profile of WIPI1 was particularly intricate, marked by a negative linkage with TRIM26 ($r = -0.69$). Additionally, IDH1, NDRG1, and TRIM26 exhibited complex patterns of both positive and negative correlations, indicating their involvement in distinct regulatory pathways (Figure 4B). Correlation analysis between these genes and twenty distinct immune cell types revealed that WIPI1 was negatively correlated with activated CD4 T cells, CD8 T cells, and dendritic cells ($p < 0.05$), but positively correlated with natural killer cells and neutrophils ($p < 0.01$). TRIM26 showed significant positive correlations with natural killer cells and dendritic cells. BID, in turn, was significantly positively correlated with specific immune cells (Figure 4C). Collectively, these correlational insights highlight the multifaceted roles of these genes in ferroptosis and immune modulation in CAD.

Clinical Studies Prove That the Differentially Expressed Gene IDH1 Can Serve as a Biomarker for CAD

To further explore the biomarkers for CAD, a clinical investigation was conducted, comprising 12 healthy controls and 26 CAD patients. Demographic analysis revealed a significantly higher mean age in the CAD cohort (69.45 ± 12.74 years) compared to controls (63.42 ± 10.39 years). Additionally, the CAD group exhibited a significantly higher prevalence of hypertension (76.9%) and diabetes (34.6%) than the control group 66.7% and 13.3%, respectively; $P < 0.05$). Body mass index (BMI) was also slightly higher in CAD patients (26.28 ± 5.13) compared to healthy controls (24.96 ± 3.15, $P < 0.05$). In terms of CAD severity, assessed by Gensini scores, the CAD group had significantly higher values (median: 22; interquartile range [IQR]: 13.4–37.5) than the control group (median: 0.0; IQR: 0.00–6.00; $P < 0.05$). No significant differences were observed between groups in gender, smoking status, or alcohol consumption ($P > 0.05$). A detailed summary of these findings is presented in Table 1.

Serum biomarker analysis revealed significantly higher levels of lactate dehydrogenase (LDH), triglycerides (TG), total cholesterol (TC), and low-density lipoprotein cholesterol (LDL-C) in CAD patients [median (interquartile range, IQR)]: LDH 176.9 (153.4–234.7) U/L, TG 2.73 (1.75–4.35) mmol/L, TC 4.95 (3.86–6.45) mmol/L, LDL-C 3.12 (2.56–3.79) mmol/L] compared to healthy controls [LDH 155.7 (141.2–162.5) U/L, TG 1.32 (1.05–1.68) mmol/L, TC 4.05 (3.72–4.69) mmol/L, LDL-C 2.37 (2.05–2.94) mmol/L], with statistically significant differences ($P < 0.05$). In contrast, white blood cell (WBC) count, alanine aminotransferase (ALT), aspartate aminotransferase (AST), and high-density lipoprotein cholesterol (HDL-C) levels were not significantly different between the CAD and control groups ($P > 0.05$), as shown in Table 2.

In an endeavor to delineate the expression patterns of six ferroptosis-associated genes—WIPI1, TRIM26, NDRG1, MMD, IDH1, and BID—in individuals with CAD, we utilized quantitative polymerase chain reaction (qPCR) to evaluate the transcriptional activity of these genes in CAD patients compared with healthy controls. Our findings revealed significant downregulation of WIPI1, TRIM26, MMD, and IDH1 expression in CAD patients compared to controls ($P < 0.05$), with IDH1 demonstrating the most substantial expression disparity between the two groups (Figure 5A–D). Conversely, the expression levels of NDRG1 and BID did not significantly differ between CAD patients and healthy controls ($P > 0.05$) (Figure 5E and F). Subsequently, CAD patients were categorized into two cohorts based on Gensini scores: a low Gensini score group (Gensini

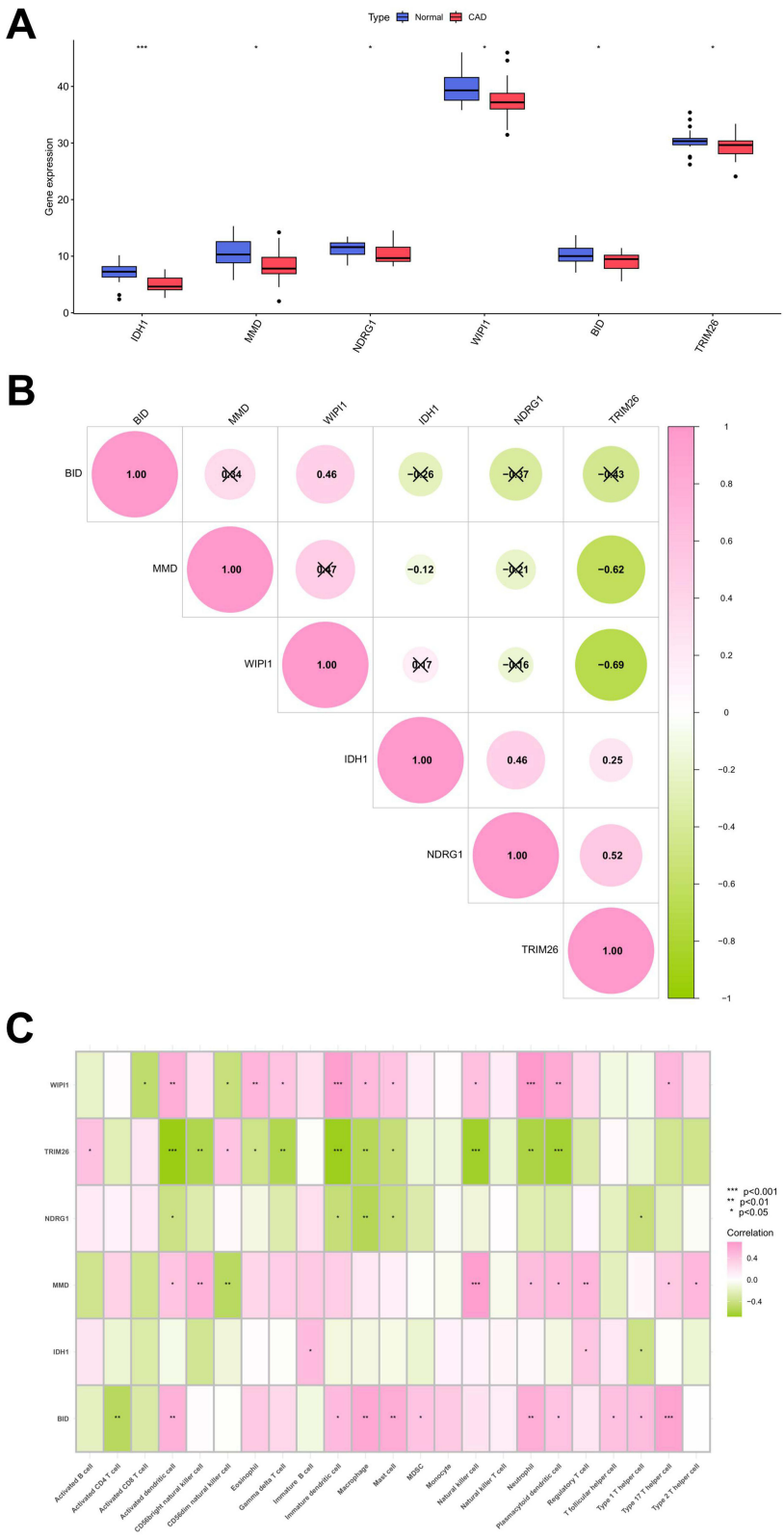

Figure 4 Analysis of peripheral immune characteristics in CAD patients. (**A**) Box plot showing significant mRNA expression differences in peripheral blood. (**B**) Correlations among Bid, MMD, WIPI1, IDH1, NDRG1, and TRIM26. (**C**) Heatmap showed the correlations between the 6 identified genes and 20 types of immune cells. Pink: Up-regulation; Green: Down-regulation. *p < 0.05, **p < 0.01, ***p < 0.001.

Table 2 Comparison of Laboratory Test Outcomes Between CAD Group and Normal Group

Variable	Normal Group (n = 12)	CAD Group (n = 26)	*P*-value
WBC (L^{-1}, × 10^9)	6.02(5.12,7.35)	6.1(4.95,7.86)	0.82
ALT (U•L)	15.60(11.67, 23.36)	16.30(12.59, 24.37)	0.768
AST (U•L)	17.25(14.25, 20.31)	17.5(14.9, 22.3)	0.316
LDH (U•L)	155.7(141.2, 162.5)	176.9(153.4, 234.7)	0.007
TG (mmol•L^{-1})	1.32(1.05, 1.68)	2.73(1.75, 4.35)	0.000
TC (mmol•L^{-1})	4.05(3.72, 4.69)	4.95(3.86, 6.45)	0.000
LDL-C (mmol•L^{-1})	2.37(2.05, 2.94)	3.12(2.56, 3.79)	0.000
HDL-C (mmol•L^{-1})	1.13(0.96, 1.25)	1.17(1.02, 1.36)	0.964
IDH1 expression	0.88(0.41, 1.37)	0.25(0.03, 0.46)	0.000

Abbreviations: WBC, White blood cell; ALT, Alanine aminotransferase; AST, Aspartate aminotransferase; LDH, Lactic dehydrogenase; TG, Triglyceride; TC, Total cholesterol; LDL-C, Low-density lipoprotein-cholesterol; HDL-C, High-density lipoprotein-cholesterol; IDH1, Isocitrate dehydrogenase 1.

score < 30, n = 10) and a high Gensini score group (Gensini score ≥ 30, n = 16). Quantitative PCR analysis showed that individuals in the low Gensini score group had markedly higher mRNA expression levels in aortic tissue than those in the high Gensini score group (Figure 6A). Furthermore, CAD patients were divided into low and high IDH1 expression groups based

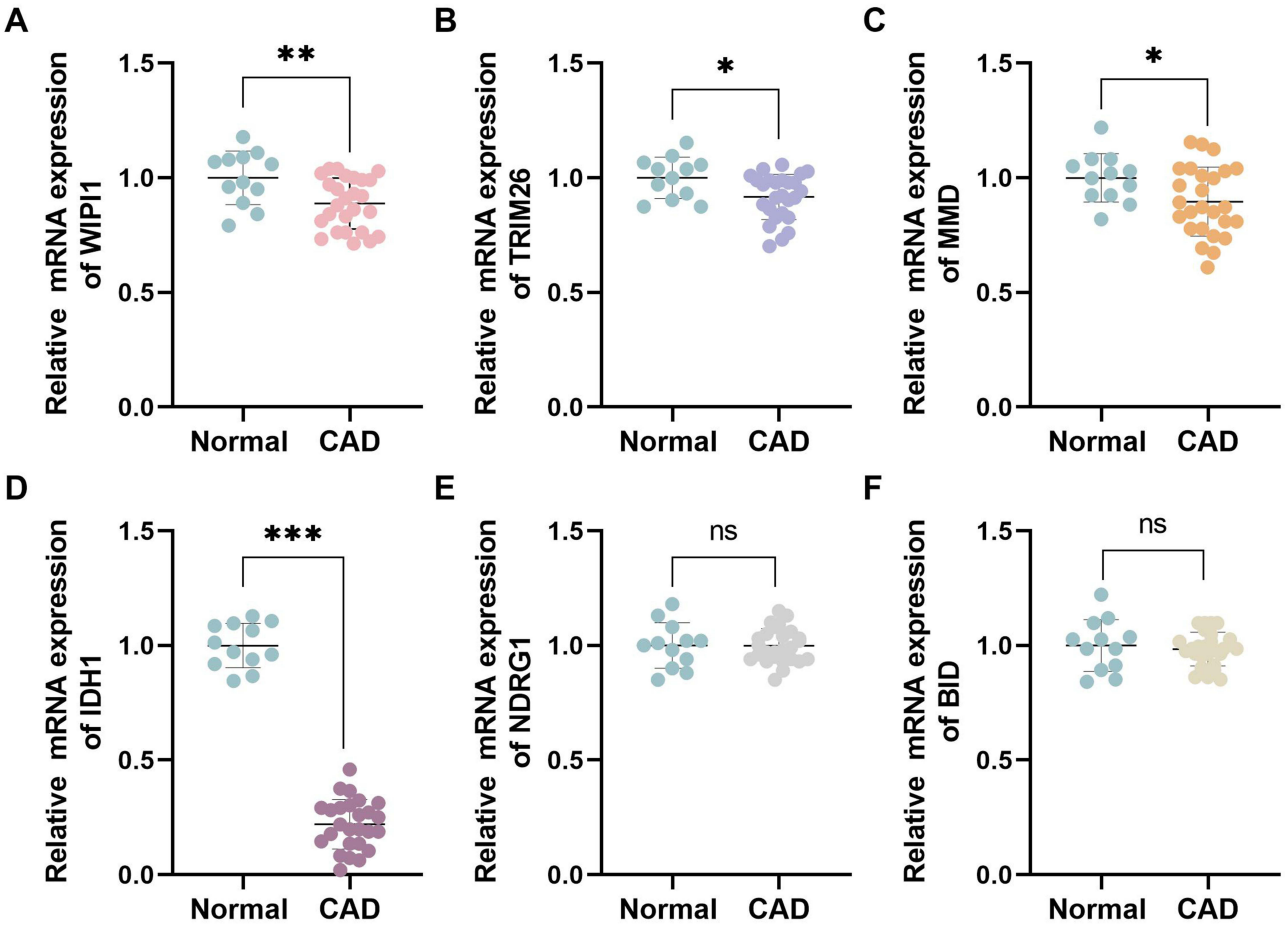

Figure 5 The expression of 6 identified genes in CAD Patients. The mRNA expression level of WIPI1 (**A**), TRIM26 (**B**), MMD (**C**), IDH1 (**D**), NDRG1 (**E**), and Bid (**F**) in CAD patients compared to healthy controls. *p < 0.05, **p < 0.01, ***p < 0.001.

https://doi.org/10.2147/IJGM.S527955

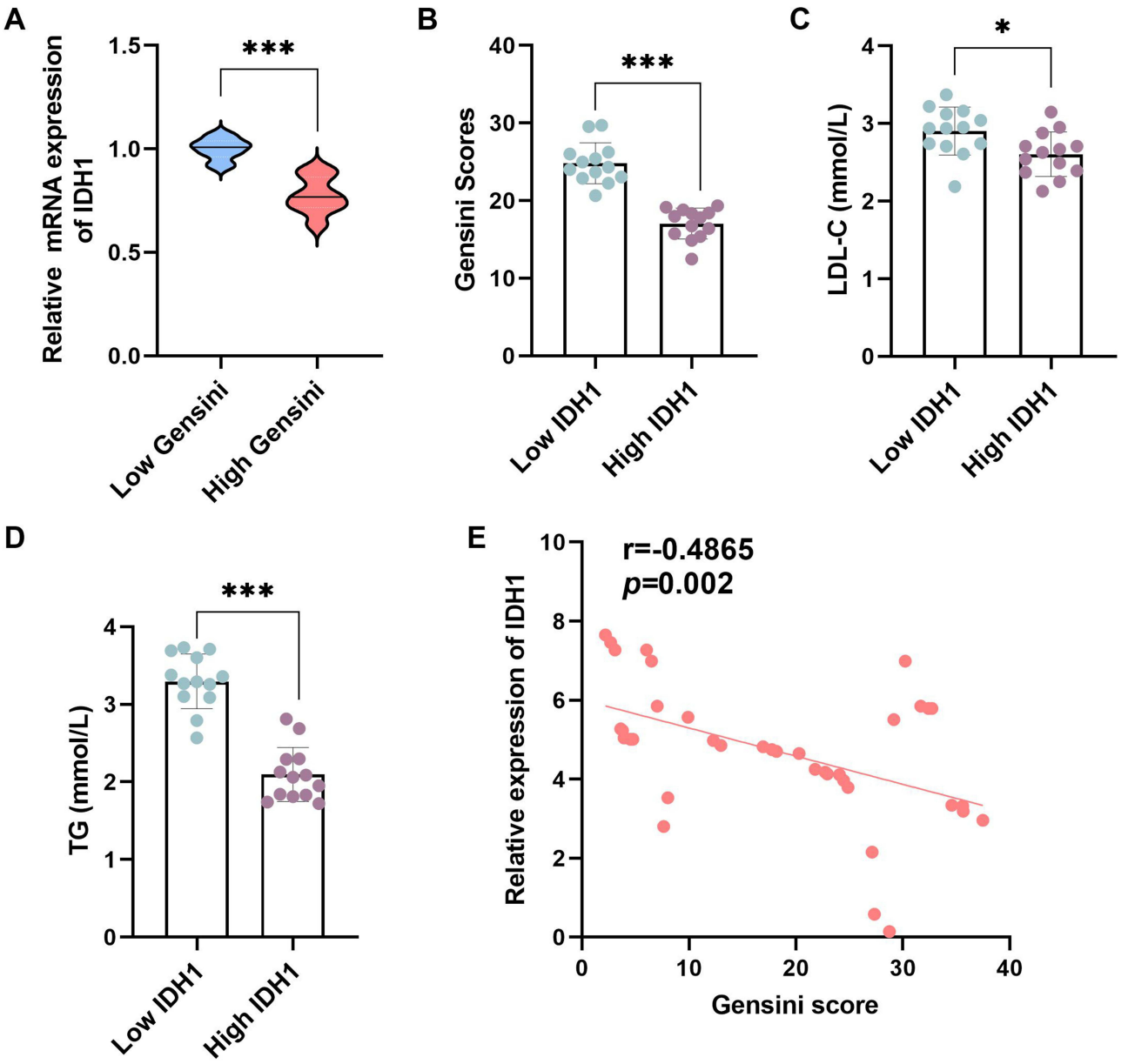

Figure 6 Clinical validation of IDH1 as a potential biomarker for CAD. (**A**) Comparison of IDH1 levels in different coronary artery lesions. (**B-D**) Comparison of Gensini score, LDL-C, TG levels between high IDH1 and low IDH1 expression groups. *p < 0.05, ***p < 0.001. (**E**) Association between IDH1 expression levels and Gensini scores.

on median IDH1 expression levels. The low IDH1 expression group exhibited a significantly higher Gensini score than the high IDH1 expression group ($P < 0.05$, Figure 6B). Laboratory assessments also showed that the low IDH1 expression group had higher levels of lipid-associated markers, including LDL-C and TG, compared to the high IDH1 expression group ($P < 0.05$, Figure 6C and D). Integrative analysis in both CAD patients and healthy controls revealed an inverse correlation between IDH1 expression levels and CAD severity, as measured by Gensini scores ($r = -0.4865$, $p = 0.002$, Figure 6E). Collectively, these results indicate that the differentially expressed gene IDH1 may serve as a promising biomarker for CAD.

Validation of IDH1 Expression in the CAD Mouse Model

To further explore the role of IDH1 in CAD, a murine model of CAD was established using 6-week-old specific pathogen-free C57BL/6J mice. Compared with sham-operated controls, CAD mice exhibited significant increases in serum total cholesterol (TC) and low-density lipoprotein cholesterol (LDL-C) levels ($P < 0.05$). Conversely, sham-operated mice had higher high-density lipoprotein cholesterol (HDL-C) levels ($P < 0.05$) (Figure 7A). Additionally, CAD

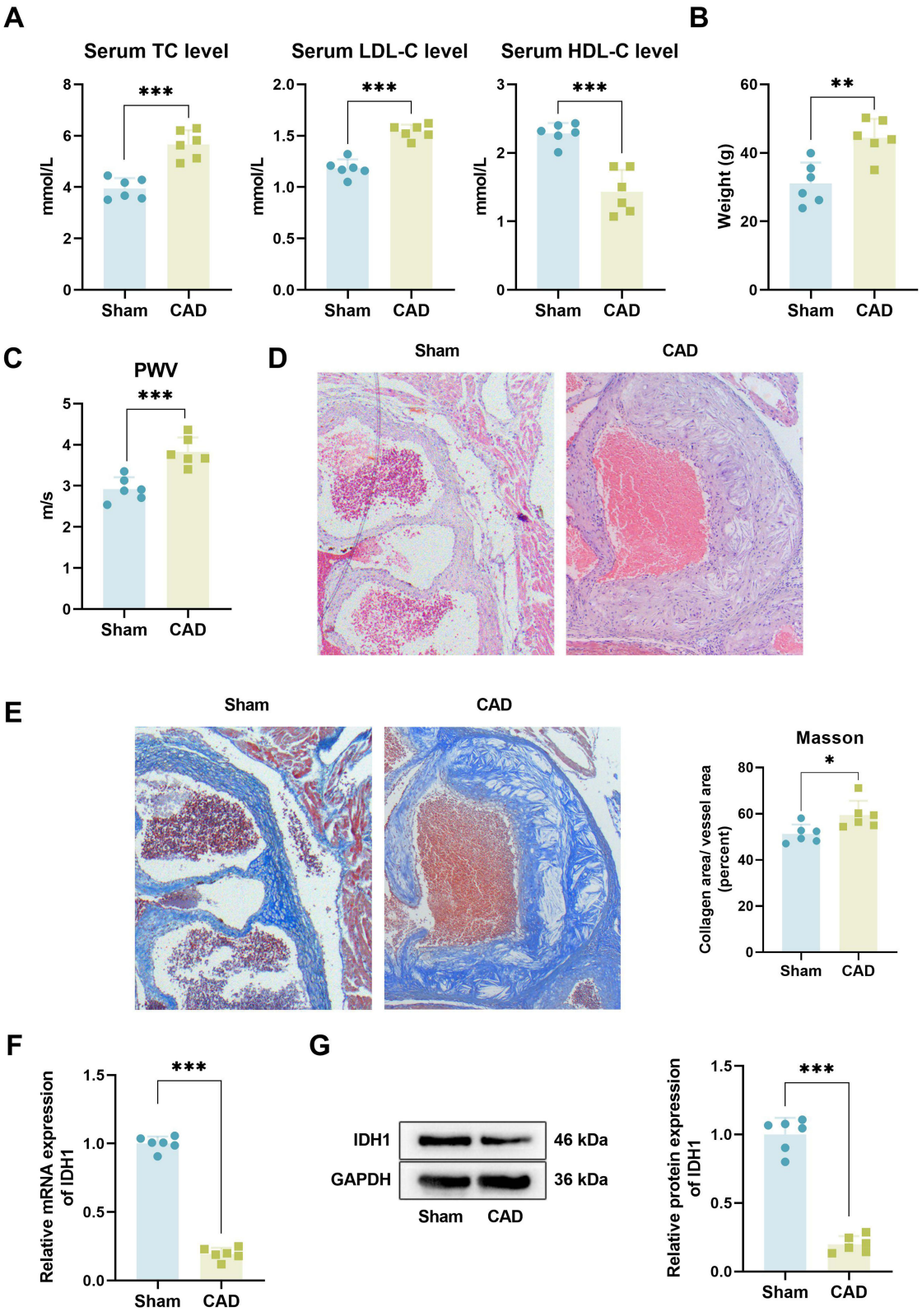

Figure 7 Validation of IDH1 expression in the CAD mouse model. (**A**) The serum concentrations of total cholesterol (TC), low-density lipoprotein cholesterol (LDL-C), and high-density lipoprotein cholesterol (HDL-C) in CAD mice compared to sham controls. (**B**) The mean body weight of CAD mice and sham controls. (**C**) The pulse wave velocity (PWV) measurements in CAD mice and sham controls. (**D**) H&E staining of aortic sections from CAD mice and sham controls. (**E**) Masson's staining of aortic sections from CAD mice and sham controls. The mRNA (**F**) and protein expression (**G**) levels of IDH1 in aortic tissues of CAD mice compared to sham controls. *p < 0.05, **p < 0.01, ***p < 0.001.

https://doi.org/10.2147/IJGM.S527955

mice showed a notable increase in mean body weight ($P < 0.05$, Figure 7B). Pulse wave velocity (PWV) measurements were performed to assess aortic stiffness revealing increased vascular rigidity in CAD mice ($P < 0.05$, Figure 7C). HE staining demonstrated that the aortic intima of the CAD mice was significantly thickened, with a large accumulation of inflammatory cells, compared to sham-operated mice (Figure 7D). Masson's staining was performed on aortic sections to evaluate collagen deposition, showing higher collagen content in the aortas of CAD mice ($P < 0.05$, Figure 7E). Collectively, these results indicate lipid deposition and vascular remodeling in CAD mice, confirming the successful establishment of the CAD model. PCR and Western blot analyses were then used to examine IDH1 expression levels in aortic tissues. As shown in Figure 7F and G, CAD mice had markedly reduced IDH1 mRNA and protein expression in aortic tissues compared to the sham group ($P < 0.05$). This finding is consistent with previous bioinformatics analyses and clinical investigations, collectively suggesting that IDH1 may serve as a potential biomarker for CAD.

Discussion

The complex pathophysiology of CAD involves intricate interactions between cellular mechanisms and signaling pathways. Ferroptosis, a form of regulated cell death, has emerged as a key player in CAD pathogenesis.[7] Iron accumulation and lipid peroxidation—hallmarks of ferroptosis—directly damage cardiomyocytes and modulate the local microenvironment to influence CAD progression. Immune regulation in CAD is dualistic: moderate immune responses aid tissue repair, while excessive activation drives chronic inflammation and atherosclerosis.[19]

Ferroptosis and immune regulation are interdependent: ferroptotic cells release damage-associated molecular patterns (DAMPs) that trigger activate the immune activation and inflammation;[10,12] while immune cell function and cytokines reciprocally affect iron metabolism and antioxidant capacity to regulate ferroptosis.[8,20] This crosstalk is central to CAD pathophysiology. Investigating this interplay enhances understanding of CAD mechanisms and identifies novel therapeutic targets. In this study, we analyze gene expression, immune cell infiltration, and ferroptosis-related gene patterns to uncover links between these processes and their diagnostic/treatment potential in CAD.

To achieve the study objectives, we obtained mRNA expression profiles of CAD patients and controls from the GEO database. Intersection analysis with ferroptosis-related genes identified 29 DEGs. GO analysis showed these genes are associated with fatty acid metabolism, inflammatory responses, and autophagy dysregulation—key processes in CAD pathogenesis that may exacerbate disease progression (Figure 3B). KEGG pathway enrichment analysis revealed DEGs were involved in ferroptosis and multiple immune-related pathways: FoxO signaling, PD-L1/PD-1 checkpoint, NOD-like receptor signaling, HIF-1 signaling, Th17 cell differentiation, and VEGF signaling (Figure 3C). The FoxO pathway regulates cell survival and metabolism; its dysregulation contributes to endothelial dysfunction and atherosclerosis.[21] PD-L1/PD-11 signaling influences T cell tolerance and correlates with ferroptosis; sPD-L1 levels are elevated in CAD patients and linked to cardiovascular events.[22,23] NOD-like receptor signaling modulates inflammation via NLRP3 inflammasome activation, promoting endothelial dysfunction and CAD progression.[24–26] Enrichment of Th17 cell differentiation and autophagy pathways further supports their role in CAD progression.[27] These findings confirm associations between ferroptosis-related DEGs and CAD-relevant biological processes and pathways, providing a basis for further mechanistic and translational research.

Immune cell activation plays a pivotal role in the progression of CAD, and single-cell RNA sequencing of immune cell phenotypes derived from peripheral blood mononuclear cells has increasingly been utilized for the diagnosis of CAD.[28] Research has demonstrated a significant elevation in the frequency of activated dendritic cells (cDC) among patients at high risk for CAD, with this increase being correlated to the severity of CAD.[29] Furthermore, clinical studies have highlighted a notable activation of neutrophils in individuals with CAD.[30] In our study, we observed a significant enrichment of dendritic cells and neutrophils within the CAD cohort (Figure 4B), a result that aligns with the findings of Feng et al, thereby providing additional evidence for the involvement of these cell types in the pathogenesis of CAD.[14]

Peripheral blood biomarkers are critical for CAD diagnosis. Using LASSO regression, we developed a diagnostic model from 29 ferroptosis-associated genes, identifying six key genes: IDH1, MMD, NDRG1, WIPI1, BID, and TRIM26. All genes showed AUC values >0.65 (Figure 5C), with IDH1 demonstrating the highest efficacy (AUC=0.821), confirming their potential to distinguish CAD patients from controls. Clinical analysis revealed higher hypertension, diabetes, and lipid markers (LDH, TG, TC, LDL-C) in CAD patients. In aortic tissues, WIPI1, TRIM26, MMD, and IDH1 were downregulated,

with IDH1 showing the most significant reduction and an inverse correlation with Gensini scores. Animal experiments supported IDH1's role in CAD. As a TCA cycle enzyme, IDH1 regulates intracellular redox balance and may influence atherosclerosis via NADPH-dependent antioxidant activity.[31,32] While Li et al showed IDH1 inhibition reduces macrophage ferroptosis and foam cell formation.[33] Our finding of IDH1 downregulation in CAD aortic tissues contrasts with this, possibly due to differences between CAD and atherosclerosis. Further studies are needed to clarify IDH1's role in CAD ferroptosis. Notably, IDH1 modulates immune responses in tumor immunology.[34,35] Our study found weak correlations with most immune cell types in CAD. Given Badder Kattih et al's report on mutant IDH1 and CAD prevalence,[36] future research should explore IDH1's dual mechanisms in CAD pathogenesis.

Beyond IDH1, WIPI1, TRIM26, and MMD show potential roles in CAD. WIPI1 (Wild-type p53-induced phosphatase 1), a serine/threonine phosphatase and regulator of autophagy-dependent ferroptosis, correlates with immune cell profiles: negatively with activated CD4/CD8 T cells and dendritic cells ($p < 0.05$), and positively with natural killer cells and neutrophils ($p < 0.01$), suggesting immune regulation involvement.[37–39] However, its role in CAD remains uninvestigated. Tripartite Motif Containing 26 (TRIM26), an E3 ubiquitin ligase, modulates ferroptosis and inflammation by degrading IRF3 and influencing M1 macrophage polarization, linking it to CAD pathogenesis.[40–42] MMD (Monocyte to Macrophage Differentiation Associated, also known as PAQR11) promotes monocyte-to-macrophage differentiation and ferroptosis in cancer but is poorly studied in CAD.[43,44] While these genes are implicated in immune modulation and CAD diagnosis, direct evidence for their causal role in CAD is lacking. Future studies should clarify their mechanistic contributions.

Relative to single-gene diagnosis, the six-gene ensemble shows superior diagnostic potential for CAD. Individual gene performance may be limited by expression variability and inter-individual differences, whereas a multi-gene model integrates multiple expression profiles to overcome single-gene constraints and provide a comprehensive view of CAD pathology, enhancing diagnostic accuracy. In this study, the six-gene diagnostic model (IDH1, MMD, NDRG1, WIPI1, BID, TRIM26) developed via LASSO regression achieved AUC > 0.75 in three datasets (GSE202625, GSE180081, GSE42148), outperforming single-gene analysis in differentiating CAD patients from controls. Future research should explore the model's early diagnostic utility. Given the asymptomatic nature of early CAD, sensitive and specific methods are critical. Monitoring these six genes in peripheral blood using digital PCR or nanotechnology-based platforms could enable non-invasive, early, and precise CAD diagnosis, facilitating timely intervention, improving outcomes, and reducing healthcare costs.

Although this investigation has illuminated the diagnostic import of genes including IDH1, WIPI1, TRIM26, and MMD in the context of CAD, the exact pathways through which these genes participate in the etiology and advancement of CAD necessitate additional scrutiny. Specifically, elucidating how these genes modulate the pathophysiological trajectories of CAD via ferroptosis and immune regulation demands rigorous inquiry. A notable limitation of this study is the relatively small sample size in clinical validation (26 CAD patients and 12 healthy controls), which may affect the generalizability of the findings. Subsequent research initiatives should consider expanding to multicenter, large-sample clinical trials to robustly validate the diagnostic potency and clinical relevance of these genes. Such multicenter approaches can counterbalance the potential biases associated with single-center studies, thus bolstering the credibility and broad applicability of the research outcomes. Furthermore, probing into the feasibility of these genes serving as therapeutic targets for CAD represents a fertile ground for future exploration. While the identified biomarkers demonstrated promising diagnostic value, the absence of comprehensive clinical covariates (eg, medication history) precludes us from fully evaluating their independence from other risk factors. This highlights the need for prospective studies with detailed data collection to validate these associations.

Another notable limitation of this study is the lack of detailed clinical data on patients' pharmacological therapies, kidney function, and certain comorbidities, which were not systematically recorded in the retrospective dataset. These missing data may introduce potential confounding factors, as medications (eg, statins) or renal dysfunction could influence both ferroptosis pathways and immune cell profiles. For example, statins might modulate lipid metabolism and impact ferroptosis-related gene expression, while reduced kidney function could alter systemic inflammation levels. Consequently, the generalizability of our findings to broader populations with diverse clinical profiles may be limited. To address these limitations, future studies should incorporate longitudinal data on pharmacological interventions, renal function metrics, and comorbidities, enabling more precise modeling of ferroptosis-immune interactions in CAD. Such approaches will enhance the translational value of our findings and facilitate the development of personalized therapeutic strategies.

Conclusion

This study identified ferroptosis-related genes (IDH1, MMD, NDRG1, WIPI1, BID, TRIM26) as potential CAD diagnostic biomarkers via machine learning, with a six-gene model showing strong diagnostic performance. Reduced IDH1 expression correlated with higher CAD severity, and altered immune cell profiles were linked to ferroptosis pathways. Limitations include retrospective design and incomplete clinical data, necessitating prospective validation with comprehensive datasets to enhance translational utility. Future research endeavors will delve deeper into the precise mechanisms by which these genes influence the pathogenesis and progression of CAD, and will also assess their viability as therapeutic targets.

Data Sharing Statement

Data is available from the corresponding author upon reasonable request.

Funding

There is no funding to report.

Disclosure

The authors declare that they have no conflicts of interest in this work.

References

1. Toval A, Bakker EA, Granada-Maia JB, et al. Exercise type and settings, quality of life, and mental health in coronary artery disease: a network meta-analysis. *Eur Heart J*. 2025;15:ehae870.
2. Khera AV, Kathiresan S. Genetics of coronary artery disease: discovery, biology and clinical translation. *Nat Rev Genet*. 2017;18(6):331–344. doi:10.1038/nrg.2016.160
3. Malakar AK, Choudhury D, Halder B, Paul P, Uddin A, Chakraborty S. A review on coronary artery disease, its risk factors, and therapeutics. *J Cell Physiol*. 2019;234(10):16812–16823. doi:10.1002/jcp.28350
4. Gaudino M, Crea F. Inflammation in coronary artery disease: which biomarker and which treatment? *Eur J Prev Cardiol*. 2019;26(8):869–871. doi:10.1177/2047487319829307
5. Medina-Leyte DJ, Zepeda-García O, Domínguez-Pérez M, González-Garrido A, Villarreal-Molina T, Jacobo-Albavera L. Endothelial dysfunction, inflammation and coronary artery disease: potential biomarkers and promising therapeutical approaches. *Int J Mol Sci*. 2021;22(8):3850. doi:10.3390/ijms22083850
6. Snaebjarnarson AS, Helgadottir A, Arnadottir GA, et al. Complex effects of sequence variants on lipid levels and coronary artery disease. *Cell*. 2023;186(19):4085–4099.e4015. doi:10.1016/j.cell.2023.08.012
7. Wu X, Qin K, Iroegbu CD, et al. Genetic analysis of potential biomarkers and therapeutic targets in ferroptosis from coronary artery disease. *J Cell Mol Med*. 2022;26(8):2177–2190. doi:10.1111/jcmm.17239
8. Jiang X, Stockwell BR, Conrad M. Ferroptosis: mechanisms, biology and role in disease. *Nat Rev Mol Cell Biol*. 2021;22(4):266–282. doi:10.1038/s41580-020-00324-8
9. Dixon SJ, Olzmann JA. The cell biology of ferroptosis. *Nat Rev Mol Cell Biol*. 2024;25(6):424–442. doi:10.1038/s41580-024-00703-5
10. Wang Y, Zhao Y, Ye T, Yang L, Shen Y, Li H. Ferroptosis signaling and regulators in atherosclerosis. *Front Cell Dev Biol*. 2021;9:809457. doi:10.3389/fcell.2021.809457
11. Ouyang S, You J, Zhi C, et al. Ferroptosis: the potential value target in atherosclerosis. *Cell Death Dis*. 2021;12(8):782. doi:10.1038/s41419-021-04054-3
12. Li C, Liu R, Xiong Z, et al. Ferroptosis: a potential target for the treatment of atherosclerosis. *Acta Biochim Biophys Sin*. 2024;56(3):331–344. doi:10.3724/abbs.2024016
13. Hong J, Li X, Hao Y, et al. The PRMT6/STAT1/ACSL1 axis promotes ferroptosis in diabetic nephropathy. *Cell Death Differ*. 2024;31(11):1561–1575. doi:10.1038/s41418-024-01357-8
14. Feng X, Zhang Y, Du M, et al. Identification of diagnostic biomarkers and therapeutic targets in peripheral immune landscape from coronary artery disease. *J Transl Med*. 2022;20(1):399. doi:10.1186/s12967-022-03614-1
15. Roy P, Orecchioni M, Ley K. How the immune system shapes atherosclerosis: roles of innate and adaptive immunity. *Nat Rev Immunol*. 2022;22(4):251–265. doi:10.1038/s41577-021-00584-1
16. Fernandez DM, Rahman AH, Fernandez NF, et al. Single-cell immune landscape of human atherosclerotic plaques. *Nat Med*. 2019;25(10):1576–1588. doi:10.1038/s41591-019-0590-4
17. Gencer S, Döring Y, Jansen Y, et al. Endothelial ACKR3 drives atherosclerosis by promoting immune cell adhesion to vascular endothelium. *Basic Res Cardiol*. 2022;117(1):30. doi:10.1007/s00395-022-00937-4
18. Cheng J, Cheng M, Lusis AJ, Yang X. Gene regulatory networks in coronary artery disease. *Curr Atheroscler Rep*. 2023;25(12):1013–1023. doi:10.1007/s11883-023-01170-7
19. Zhao TX, Mallat Z. Targeting the immune system in atherosclerosis: JACC state-of-the-art review. *J Am Coll Cardiol*. 2019;73(13):1691–1706. doi:10.1016/j.jacc.2018.12.083

20. Yang Y, Wang Y, Guo L, Gao W, Tang TL, Yan M. Interaction between macrophages and ferroptosis. *Cell Death Dis*. 2022;13(4):355. doi:10.1038/s41419-022-04775-z
21. Liu J, Yi X, Tao Y, Wang Y, Xu Z. Insulin-receptor substrate 1 protects against injury in endothelial cell models of ox-LDL-induced atherosclerosis by inhibiting ER stress/oxidative stress-mediated apoptosis and activating the Akt/FoxO1 signaling pathway. *Int J Mol Med*. 2020;46(5):1671–1682. doi:10.3892/ijmm.2020.4728
22. Ping Y, Shan J, Qin H, et al. PD-1 signaling limits expression of phospholipid phosphatase 1 and promotes intratumoral CD8(+) T cell ferroptosis. *Immunity*. 2024;57(9):2122–2139.e2129. doi:10.1016/j.immuni.2024.08.003
23. Miyazaki S, Fujisue K, Yamanaga K, et al. Prognostic significance of soluble PD-L1 on cardiovascular outcomes in patients with coronary artery disease. *J Atheroscler Thromb*. 2024;31(4):355–367. doi:10.5551/jat.64183
24. Sundaram B, Tweedell RE, Prasanth Kumar S, Kanneganti TD. The NLR family of innate immune and cell death sensors. *Immunity*. 2024;57(4):674–699. doi:10.1016/j.immuni.2024.03.012
25. Bai B, Yang Y, Wang Q, et al. NLRP3 inflammasome in endothelial dysfunction. *Cell Death Dis*. 2020;11(9):776. doi:10.1038/s41419-020-02985-x
26. Hemenway G, Frishman WH. Therapeutic implications of NLRP3-mediated inflammation in coronary artery disease. *Cardiol Rev*. 2022;30(2):90–99. doi:10.1097/CRD.0000000000000391
27. He T, Muhetaer M, Wu J, et al. Immune cell infiltration analysis based on bioinformatics reveals novel biomarkers of coronary artery disease. *J Inflamm Res*. 2023;16:3169–3184. doi:10.2147/JIR.S416329
28. Kott KA, Vernon ST, Hansen T, et al. Single-cell immune profiling in coronary artery disease: the role of state-of-the-art immunophenotyping with mass cytometry in the diagnosis of atherosclerosis. *J Am Heart Assoc*. 2020;9(24):e017759. doi:10.1161/JAHA.120.017759
29. Chatterjee N, Komaravolu RK, Durant CP, et al. Single cell high dimensional analysis of human peripheral blood mononuclear cells reveals unique intermediate monocyte subsets associated with sex differences in coronary artery disease. *Int J Mol Sci*. 2024;25(5):2894. doi:10.3390/ijms25052894
30. Talmor N, Pillinger MH, Xia Y, Leonard A, Curovic F, Shah B. Neutrophil activation and adhesiveness in coronary artery disease: results from the COLCHICINE-PCI biomarker substudy. *J Am Heart Assoc*. 2024;13(19):e036701. doi:10.1161/JAHA.124.036701
31. Liu X, Gong Y. Isocitrate dehydrogenase inhibitors in acute myeloid leukemia. *Biomark Res*. 2019;7:22. doi:10.1186/s40364-019-0173-z
32. Itsumi M, Inoue S, Elia AJ, et al. Idh1 protects murine hepatocytes from endotoxin-induced oxidative stress by regulating the intracellular NADP(+)/NADPH ratio. *Cell Death Differ*. 2015;22(11):1837–1845. doi:10.1038/cdd.2015.38
33. Li B, Wang C, Lu P, et al. IDH1 promotes foam cell formation by aggravating macrophage ferroptosis. *Biology*. 2022;11(10):1392. doi:10.3390/biology11101392
34. Lai K, Chen Z, Lin S, et al. The IDH1-R132H mutation aggravates cisplatin-induced acute kidney injury by promoting ferroptosis through disrupting NDUFA1 and FSP1 interaction. *Cell Death Differ*. 2024;32(2):242–255. doi:10.1038/s41418-024-01381-8
35. Zhu Y, Kwong LN. IDH1 inhibition reawakens the immune response against cholangiocarcinoma. *Cancer Discov*. 2022;12(3):604–605. doi:10.1158/2159-8290.CD-21-1643
36. Kattih B, Shirvani A, Klement P, et al. IDH1/2 mutations in acute myeloid leukemia patients and risk of coronary artery disease and cardiac dysfunction-a retrospective propensity score analysis. *Leukemia*. 2021;35(5):1301–1316. doi:10.1038/s41375-020-01043-x
37. Sporbeck K, Haas ML, Pastor-Maldonado CJ, Schüssele DS, Hunter C, Takacs Z. The ABL-MYC axis controls WIPI1-enhanced autophagy in lifespan extension. *Commun Biol*. 2023;6(1):872. doi:10.1038/s42003-023-05236-9
38. Liao CC, Ho MY, Liang SM, Liang CM. Recombinant protein rVP1 upregulates BECN1-independent autophagy, MAPK1/3 phosphorylation and MMP9 activity via WIPI1/WIPI2 to promote macrophage migration. *Autophagy*. 2013;9(1):5–19. doi:10.4161/auto.22379
39. Liu S, Zhai J, Li D, Peng Y, Wang Y, Dai B. Identification and validation of molecular subtypes' characteristics in bladder urothelial carcinoma based on autophagy-dependent ferroptosis. *Heliyon*. 2023;9(11):e21092. doi:10.1016/j.heliyon.2023.e21092
40. Wang Z, Xia Y, Wang Y, et al. The E3 ligase TRIM26 suppresses ferroptosis through catalyzing K63-linked ubiquitination of GPX4 in glioma. *Cell Death Dis*. 2023;14(10):695. doi:10.1038/s41419-023-06222-z
41. Wang P, Zhao W, Zhao K, Zhang L, Gao C. TRIM26 negatively regulates interferon-β production and antiviral response through polyubiquitination and degradation of nuclear IRF3. *PLoS Pathog*. 2015;11(3):e1004726. doi:10.1371/journal.ppat.1004726
42. Li T, Zhong W, Li M, et al. TRIM26 deficiency enhancing liver regeneration through macrophage polarization and β-catenin pathway activation. *Cell Death Dis*. 2024;15(6):453. doi:10.1038/s41419-024-06798-0
43. Phadnis VV, Snider J, Varadharajan V, et al. MMD collaborates with ACSL4 and MBOAT7 to promote polyunsaturated phosphatidylinositol remodeling and susceptibility to ferroptosis. *Cell Rep*. 2023;42(9):113023. doi:10.1016/j.celrep.2023.113023
44. Lin Y, Huang M, Wang S, You X, Zhang L, Chen Y. PAQR11 modulates monocyte-to-macrophage differentiation and pathogenesis of rheumatoid arthritis. *Immunol Cell Biol*. 2021;163(1):60–73.